Symmetry-Breaking Bifurcation of Radially Outgoing Flow between Two Disks (Generation-Sustenance Mechanism and Statistical Law of Turbulence)

AUTHOR(S):

Mizushima, Jiro; Tanaka, Hidekazu

数理解析研究所講究録 1285 巻 2002 年 122-129

Symmetry-Breaking Bifurcation of Radially Outgoing Flow between Two Disks

同志社大・工 水島二郎 (Jiro MIZUSHIMA) 田中秀和 (Hidekazu TANAKA)
Department of Mechanical Engineering,
Doshisha University

1. Introduction

Radially outgoing flow between two parallel circular disks is a simple model for flows in the injection molding of plastic, hydrostatic air bearings and centrifugal compressor diffusers. The local Reynolds number defined by using the half distance between two circular disks and the local representative velocity decreases as the flow goes downstream between two disks.

Appearance of separation vortices in the flow field was reported by Ishizawa[1,2], that is explained by the presence of an adverse pressure gradient at small radii. He analyzed the flow by applying the boundary layer theory with a series-expansion method for the inlet region and with a momentum-integral method for the downstream region on the assumption of symmetric flow field, and predicted the threshold Reynolds number Re_t for the appearance of the separation vortices as $Re_t \sim 100$. It is added that Ishizawa assumed a uniform flow at the inlet section and the non-dimensional inlet radius, the ratio of the inlet radius to the half width between two disks, being unity. The separation vortices were also found to appear in the numerical results by Raal[3] who made numerical calculations of the steady-state solution by using finite difference approximation on the assumption of symmetric flow field along the center line between two disks for the same flow field as Ishizawa treated. However, the value of the throshold Reynolds number evaluated by Raal is 60, which differs significantly from the value $Re_t \sim 100$ predicted by Ishizawa.

Mochizuki and Yang[4] investigated the instability of the flow numerically and experimentally. The flow-visualization method was employed in their experiments and the dynamical vorticity transport equations were solved by using finite difference approximation without assuming the symmetry along the centerline between two disks in numerical simulations. They observed oscillatory flows above a critical Reynolds number, and evaluated the value of the critical Reynolds number numerically and experimentally, where a good accordance between numerical and experimental evaluations was shown. The non-dimensional inlet radius they adopted is 13.3, which differs from the value of Ishizawa or Raal. So, the direct comparison of the results obtained by Mochizuki and Yang with those by Ishizawa and Raal is difficult. However, it is concluded that the flow field is symmetric below the critical Reynolds number and the flow becomes oscillatory, which inevitably accompanies asymmetric flow fields.

Instability of radial outgoing flow between two parallel circular disks and its transition is investigated by numerical simulations and the linear stability analysis in the present paper. We adopt the same configuration of the problem with Ishizawa[1,2] and Raal.[3] The effect of the value of the non-dimensional inlet radius on the transition of flow is also considered. Axisymmetric incompressible flow field is assumed, but the symmetry along the centerline between two disks is not assumed. An analysis of the asymptotic solution in the far field from the center is also given.

2. Formulation

Consider a radially outgoing flow between two parallel circular disks with the spacing $2h^*$ and the infinite outer radius (Fig. 1). Flow enters into the gap between the two disks from the inlet AB at the

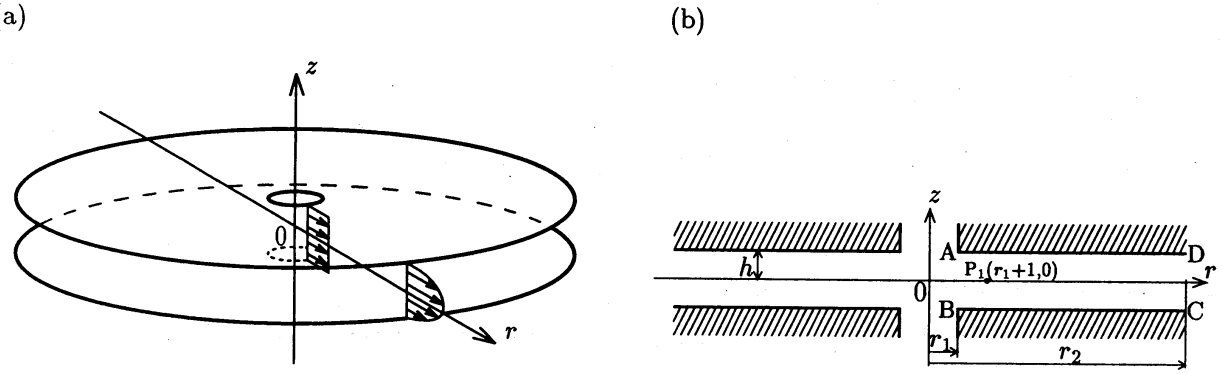

Fig. 1 Configuration and coordinates.

inner radius r_1^* with a uniform velocity profile. We define two non-dimensional parameters, i.e., the Reynolds number and the non-dimensional inlet radius, as

$$Re \equiv \frac{Q^*}{4\pi\nu h^*}, \quad r_1 \equiv r_1^*/h^*, \tag{1}$$

where Q^* is the volumetric flow rate through the gap between two disks and ν is the kinematic viscosity of the fluid.

2.1 Fundamental equation

We introduce the stream function $\psi(r,z,t)$ for the axisymmetric flow in the cylindrical coordinates. The governing equations for the vorticity component $\omega(r,z,t)$ in the circumferential direction and the stream function $\psi(r,z,t)$ are written in a non-dimensional form as

$$\frac{\partial\omega}{\partial t} - \frac{1}{r}\frac{\partial(\psi,\omega)}{\partial(r,z)} - \frac{1}{r^2}\frac{\partial\psi}{\partial z}\omega = \frac{1}{Re}\Delta\omega, \tag{2}$$

$$\omega = \frac{1}{r}D^2\psi, \tag{3}$$

where

$$\frac{\partial(f,g)}{\partial(r,z)} \equiv \frac{\partial f}{\partial r}\frac{\partial g}{\partial z} - \frac{\partial f}{\partial z}\frac{\partial g}{\partial r}, \quad \Delta \equiv \frac{\partial^2}{\partial r^2} + \frac{1}{r}\frac{\partial}{\partial r} + \frac{\partial^2}{\partial z^2} - \frac{1}{r^2}, \quad D^2 \equiv \frac{\partial^2}{\partial r^2} - \frac{1}{r}\frac{\partial}{\partial r} + \frac{\partial^2}{\partial z^2},$$

and all the physical variables are made non-dimensional by using the representative length h^* and the representative velocity $Q^*/4\pi h^{*2}$.

The flow is assumed to enter the inlet (AB in Fig. 1) with a uniform velocity profile so that the boundary condition is written as

$$\psi = z, \quad \omega = 0, \quad (r = r_1). \tag{4}$$

The boundary condition at the two disks is the nonslip boundary condition that is expressed by

$$\psi = \pm 1, \quad \omega = \frac{1}{r}\frac{\partial^2\psi}{\partial z^2}, \quad (z = \pm 1), \tag{5}$$

where the complex signs are taken in the same order. The flow field is assumed to extend to infinitely large radius, therefore the flow field has the asymptotic velocity at sufficiently large distance from the center, which is derived in the next subsection. Then the boundary condition at the end of computational domain (CD in Fig. 1) is expressed as

$$\psi = \frac{1}{2}(3z - z^3) + \frac{3}{8Re}\left(\frac{1}{7}z - \frac{11}{35}z^3 + \frac{1}{5}z^5 - \frac{1}{35}z^7\right)\frac{1}{r^2},$$
$$\omega = \frac{3}{Re}\left(\frac{1}{7}z - \frac{11}{35}z^3 + \frac{1}{5}z^5 - \frac{1}{35}z^7\right)\frac{1}{r^5} - 3\frac{z}{r} + \frac{3}{4Re}\left(-\frac{33}{35}z + 2z^3 - \frac{3}{5}z^5\right)\frac{1}{r^3},$$
$$(r = r_2). \quad (6)$$

2.2 Asymptotic solution for far field

It is expected that the outgoing flow between two disks approaches to the fully developed plane Poiseuille flow far downstream. We make an asymptotic analysis to derive the profile of the flow field at far distance. A new variable defined by

$$\xi = \frac{1}{r}, \quad (7)$$

is introduced, then the flow region is transformed from $r = [r_1, \infty)$ to $\xi = [0, 1/r_1]$. Steady flow field is assumed at very far distance, therefore Eqs. (2) and (3) are rewritten as

$$\xi^3 \frac{\partial \psi}{\partial \xi}\frac{\partial}{\partial z}\Lambda\psi - \xi^3 \frac{\partial}{\partial \xi}\Lambda\psi - \xi^2 \frac{\partial \psi}{\partial z}\Lambda\psi = \frac{1}{Re}\Lambda^2\psi, \quad (8)$$

at far downstream, where

$$\Lambda = \xi^4 \frac{\partial^2}{\partial \xi^2} + 3\xi^2 \frac{\partial}{\partial \xi} + \frac{\partial^2}{\partial z^2}.$$

We explore the solution $\psi(\xi, z)$ of Eq. (8) in a series of expansion in $\xi(= 1/r)$ expressed as

$$\psi(\xi, z) = \psi_0 + \xi\psi_1 + \xi^2\psi_2 + O(\xi^3), \quad (9)$$

where only the terms up to $O(\xi^2)$ are retained. The boundary conditions for the expansion coefficients ψ_n are written as

$$\psi_0 = \pm 1, \qquad \frac{\partial \psi_0}{\partial z} = 0, \qquad (z = \pm 1),$$
$$\psi_n = 0, \qquad \frac{\partial \psi_n}{\partial z} = 0, \qquad (z = \pm 1), \quad (10)$$

where the complex signs should be taken in the same order and n should taken to be 1 or 2. By substituting the expansion (9) into Eq. (8) and equating the terms with the same power of ξ, we obtain the equations for ψ_n, $(n = 0, 1, 2)$. After solving the resultant equation for ψ_n, we obtain the asymptotic expression of ψ at large distance as expressed as

$$\psi(r, z) = \frac{1}{2}(3z - z^3) + \frac{3}{8Re}\left(\frac{1}{7}z - \frac{11}{35}z^3 + \frac{1}{5}z^5 - \frac{1}{35}z^7\right)\frac{1}{r^2}. \quad (11)$$

where the solutions are expressed in r by substituting $r = 1/\xi$. The asymptotic solution (11) is adopted as the boundary condition for our numerical simulations and the numerical calculations of the steady and symmetric solutions.

2.3 Steady and symmetric solution

Steady and symmetric solution along the centerline between two disks exists regardless of the magnitude of the Reynolds number, which is unstable at the Reynolds numbers above a critical value. The steady and symmetric solution $(\bar{\psi}, \bar{\omega})$ satisfies the steady-state equations, which are obtained by dropping the terms with time derivative $\partial/\partial t$ in Eq. (2).

The steady and symmetric solution can be calculated in the upper or lower half domain of ABCD in Fig. 1, therefore the boundary condition on the centerline between the two disks is expressed as

$$\bar{\psi} = 0, \quad \bar{\omega} = 0, \quad (z = 0). \tag{12}$$

The boundary conditions for $(\bar{\psi}, \bar{\omega})$ at the inlet $r = r_1$, the outlet $r = r_2$ and the top or the bottom disks are the same as that of Eqs. (2) and (3).

2.4 Disturbance equation

We consider a disturbance (ψ', ω') added to the steady and symmetric solution $(\bar{\psi}, \bar{\omega})$ and express the stream function and the vorticity (ψ, ω) as $\psi = \bar{\psi} + \psi'$ and $\omega = \bar{\omega} + \omega'$ to investigate the stability of the steady and symmetric solution. The linear disturbance equations are obtained by substituting the expressions for $\psi = \bar{\psi} + \psi'$ and $\omega = \bar{\omega} + \omega'$ into Eqs. (2) and (3), subtracting the steady-state equations, and neglecting the higher order terms than the linear terms concerning the disturbance ψ' and ω'. Furthermore, the solution (ψ', ω') can be shown to have the form of $\psi' = \hat{\psi}\exp(\lambda t)$, and $\omega' = \hat{\omega}\exp(\lambda t)$, then substitution of these expression into (ψ', ω') leads the equations for $(\hat{\psi}, \hat{\omega})$ as

$$\lambda\hat{\omega} - \frac{1}{r}\left\{\frac{\partial\bar{\psi}}{\partial r}\frac{\partial\hat{\omega}}{\partial z} + \frac{\partial\hat{\psi}}{\partial r}\frac{\partial\bar{\omega}}{\partial z} - \frac{\partial\bar{\psi}}{\partial z}\frac{\partial\hat{\omega}}{\partial r} - \frac{\partial\hat{\psi}}{\partial z}\frac{\partial\bar{\omega}}{\partial r}\right\} - \frac{1}{r^2}\left\{\frac{\partial\bar{\psi}}{\partial z}\hat{\omega} + \frac{\partial\hat{\psi}}{\partial z}\bar{\omega}\right\} = \frac{1}{Re}\Delta\hat{\omega}, \tag{13}$$

$$\hat{\omega} = \frac{1}{r}D^2\hat{\psi}. \tag{14}$$

The boundary conditions for $(\hat{\psi}, \hat{\omega})$ are written as

$$\begin{aligned} &\hat{\psi} = 0, && \hat{\omega} = 0, && (r = r_1, r_2), \\ &\hat{\psi} = 0, && \hat{\omega} = \frac{1}{r}\frac{\partial^2\hat{\psi}}{\partial z^2}, && (z = \pm 1). \end{aligned} \tag{15}$$

The disturbance equation can be solved in the upper or lower half domain of ABCD in Fig. 1, therefore the boundary condition on the centerline between the two disks is expressed as

$$\hat{\psi}(r, z) = \hat{\psi}(r, -z), \quad \hat{\omega}(r, z) = \hat{\omega}(r, -z), \quad (z = 0). \tag{16}$$

3. Numerical method

3.1 Numerical simulation

In numerical simulations by the time marching method, an equally spaced mesh system with $\Delta r = \Delta z = 5 \times 10^{-2}$ is used. The vorticity transport equation is solved by the Runge-Kutta method with the fourth-order accuracy in time together with the second-order accuracy of central finite difference in space. The time increment Δt is chosen as $\Delta t = 1 \times 10^{-4}$. The Poisson equation is discretized by the second-order central finite difference and solved by the SOR method, where the relaxation factor ϵ is taken as $\epsilon = 1.82$.

3.2 Steady and symmetric solution and linear stability analysis

Both the steady-state vorticity transport equation and the Poisson equation are solved by the SOR iterative method to calculate steady and symmetric solutions. Spatial derivatives are approximated by the second-order finite differences. The relaxation factor ϵ for the SOR method is determined by considering the aspect ratio and the Reynolds number in the range $0.1 < \epsilon < 1.0$. In order to calculate unstable steady and symmetric solutions above a critical Reynolds number, the SOR method is utilized under the symmetry condition along the centerline between two disks. This method is used also for the numerical evaluation of the linear growth rate.

4. Numerical results

4.1 Flow patterns and bifurcation

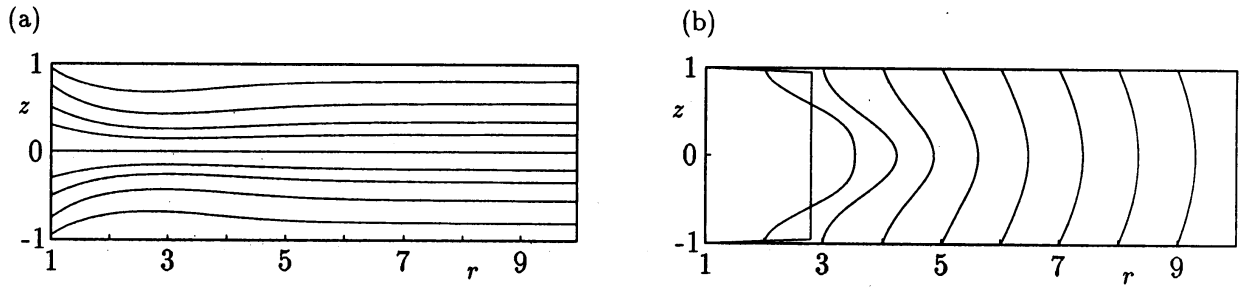

Fig. 2 Flow pattern. $Re = 40, r_1 = 1$. (a) Streamlines. (b) Velocity profiles.

For the case of the non-dimensional inlet radius $r_1 = 1$, we have done numerical simulations for the Reynolds numbers in the range of $10 \leq Re \leq 200$. The outgoing flow is symmetric at small Reynolds numbers. A typical example of such a steady and symmetric flow is shown in Fig. 2 for $Re = 40$. Streamlines for the symmetric flow is depicted in Fig. 2 (a) and the velocity profiles in the z-direction is shown in Fig. 2 (b). The streamlines gather together just downstream of the inlet as seen in Fig. 2 (a), where jet-like flow is observed in Fig. 2 (b). Another flow pattern shown in Fig. 3 ($Re = 50$) is also a steady and symmetric flow, but differs from that in Fig. 2 in presence of separation vortices. The separation vortices in Fig. 3 (a) are formed lying in $r = 1.85 - 3.55$ near both the upper and lower walls.

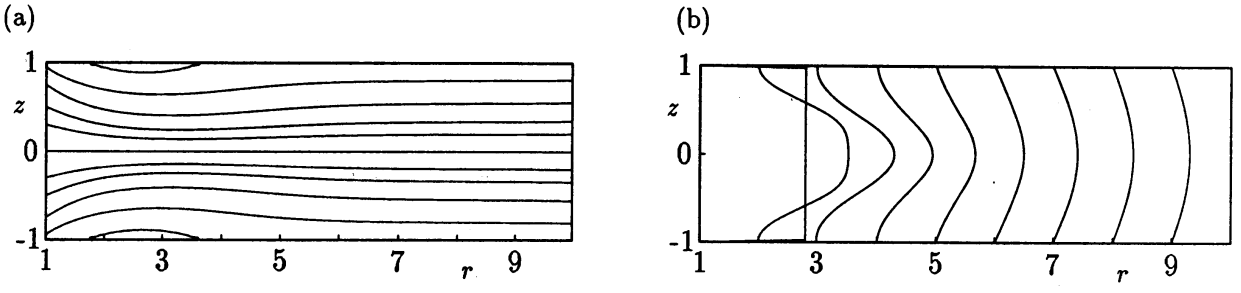

Fig. 3 Flow pattern. $Re = 50, r_1 = 1$. (a) Streamlines. (b) Velocity profiles.

The flow pattern obtained in numerical simulations at $Re = 70$ is steady, but asymmetric as depicted in Fig. 4. The stream coming from the inlet is seen to bend on the lower wall. We can easily imagine another asymmetric flow, which bends on the upper wall from the symmetry consideration of the system. Such a steady and asymmetric flow has not been reported before. The separation-vortex region in Fig. 4

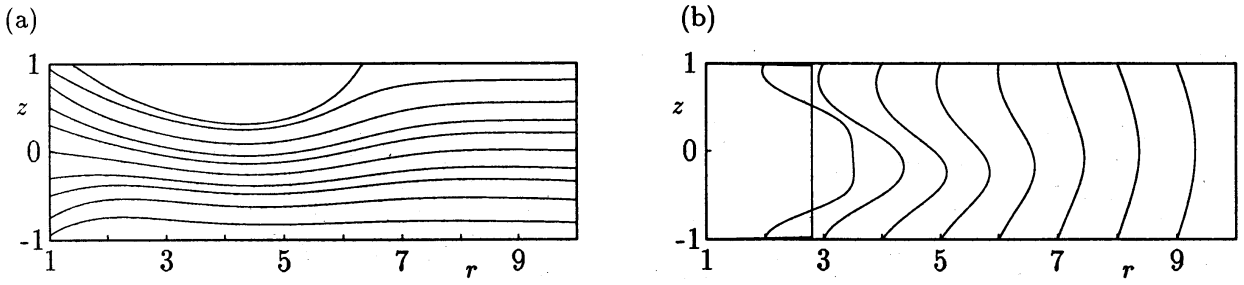

Fig. 4 Flow pattern. $Re = 70, r_1 = 1$. (a) Streamlines. (b) Velocity profiles.

(a) is larger than that in Fig. 3 (a), and the separation vortex lies in $r = 1.5 - 6.3$ near the upper wall.

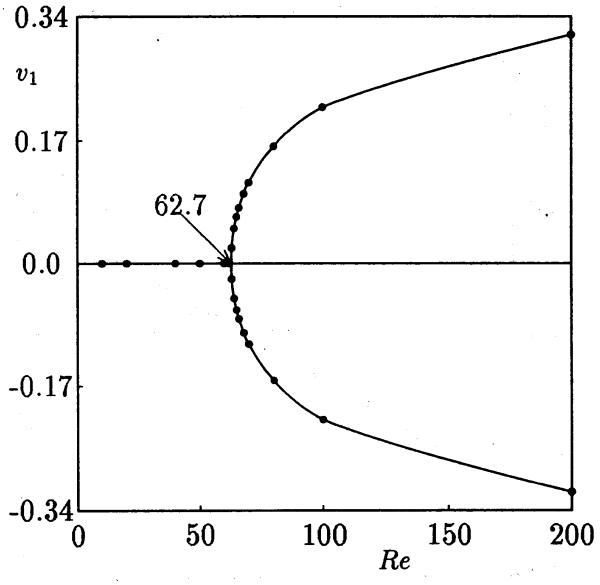

Fig. 5 Bifurcation diagram, $r_1 = 1$.

We have confirmed by numerical calculations of the steady-state equations that the symmetric flow also does exist at $Re = 70$. The asymmetric flow is thought to appear due to the instability of the symmetric flow. In order to investigate the bifurcation of steady-state solution, we obtain the bifurcation diagram by adopting a representation value v_1, the velocity in z-direction at a representation point P_1 [$(r, z) = (2, 0)$,Fig. 1]. The bifurcation diagram is depicted in Fig. 5. The bifurcation is determined as a pitchfork bifurcation from the relation ${v_1}^2 \propto (Re - Re_c)$, and the critical Reynolds number Re_c being 62.7.

4.2 Linear stability analysis

We investigate the linear stability of the steady and symmetric solution which is a basic solution of the outgoing flow for the case of the non-dimensional inlet radius $r_1 = 1$. We have solved the steady-state equations numerically to obtain the steady and symmetric solutions $(\bar{\psi}, \bar{\omega})$ and also solved Eqs. (13) and (14) to evaluate the linear growth rate λ for the steady and symmetric solutions. Typical examples of a steady and symmetric flow and a linear disturbance are shown in Fig. 6 for the Reynolds number $Re = 64$. Figure 6 (a) shows the streamlines of the steady and symmetric solution, and the disturbance obtained by solving Eqs. (13) and (14) is depicted in Fig. 6 (b). The disturbance has significant magnitude in a

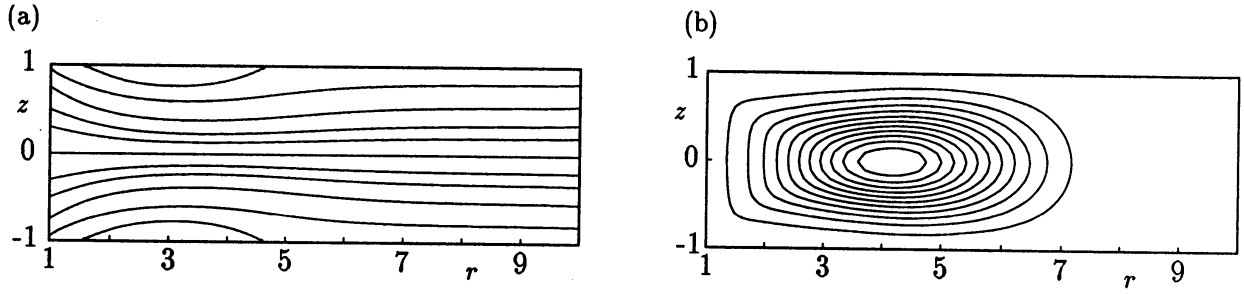

Fig. 6 Flow pattern. $Re = 64, r_1 = 1$. Streamlines. (a) Unstable symmetric flow. (b) Disturbance.

limited region near the inlet, which makes the symmetric flow to bend on one wall in that region.

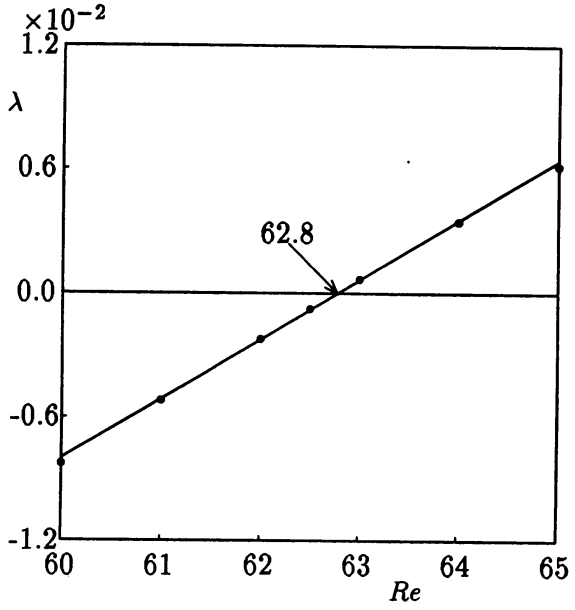

Fig. 7 Linear growth rate λ, $r_1 = 1$.

The linear growth rate λ is evaluated for various Reynolds numbers, which is shown in Fig. 7 for the non-dimensional inlet radius $r_1 = 1$. The critical Reynolds number Re_c is determined as $Re_c = 62.8$ from Fig. 7 for the non-dimensional inlet radius $r_1 = 1$. The relative error between the values of $Re_c = 62.7$ obtained from the bifurcation diagram and $Re_c = 62.8$ from the linear stability analysis is about 0.16%, which shows the consistency between the two values.

We have evaluated the critical Reynolds number Re_c for others values of the non-dimensional inlet radus r_1 and depicted them against r_1 in Fig. 8 in the range of $0.5 \leq r_1 \leq 3$. The flow is symmetric at the Reynolds number under the solid line in Fig. 8, but becomes asymmetric at the Reynolds number above the line. The steady and asymmetric flow may make a transition into an oscillatory flow above another Reynolds number, say Re_c'. However, it may be possible that the steady and symmetric flow makes a transition into an oscillatory flow without experiencing an asymmetric flow for the non-dimensional inlet radii r_1 much larger than 3. The critical Reynolds number Re_c' may approach to 5771, where the plane Poiseuille flow becomes unstable.

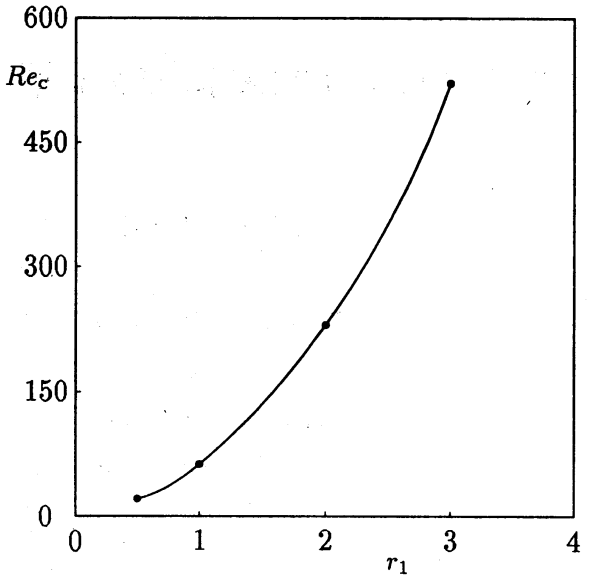

Fig. 8 Critical Reynolds number and r_1 : the non-dimensional inlet radus.

5. Conclusions

We made an asymptotic analysis for the flow profile at far distance and confirmed the flow field approaches to the fully developed plane Poiseuille flow there. We have done numerical simulations, numerical calculations of the steady symmetric solutions and their linear stability analysis for the outgoing flow with finite difference approximations. As results, we found that the flow is symmetric at small Reynolds numbers, but becomes asymmetric above a critical Reynolds number. The transition into the asymmetric flow is determined due to a pitchfork bifurcation judging from the relation ${v_1}^2 \propto (Re - 62.7)$ for the non-dimensional inlet radius $r_1 = 1$. The critical Reynolds number obtained from the linear stability analysis is 62.8, which is in good agreement with the critical value 62.7 evaluated by numerical simulation data. The larger the value of the non-dimensional inlet radii r_1 is, the larger the value of the critical Reynolds numbers Re_c for a transition into asymmetric flow becomes.

References

1) S. Ishizawa, Bulletin of JSME, **8**, 353-367 (1965).

2) S. Ishizawa, Bulletin of JSME, **9**, 86-103 (1966).

3) J. D. Raal, J. Fluid Mech., **85**, 401-416 (1978).

4) S. Mochizuki and W. J. Yang, J. Fluid Mech., **154**, 377-397 (1985).